Depositional architecture and structural evolution of a region immediately inboard of the locus of continental breakup (Liwan Sub-basin, South China Sea)

Chao Lei[12], Tiago M.Alves[3], Jianye Ren[12], Xiong Pang[4], Linlong Yang[2], Jun Liu[4]

[1] *Key laboratory of Tectonics and Petroleum Resources of Ministry of Education, China University of Geosciences, Wuhan 430074, China*
[2] *College of Marine Science and Technology, China University of Geosciences, Wuhan 430074, China*
[3] *3D Seismic Lab, School of Earth and Ocean Sciences, Cardiff University, Main Building, Park Place, Cardiff, CF10 3AT, United Kingdom*
[4] *China National Offshore Oil Corporation Ltd., Guangzhou 510240, China*

Abstract

New 3D seismic data and regional 2D seismic profiles from the northern South China Sea, the most extensive dataset imaging a distal rifted margin in the world, are used to characterize a region located immediately inboard of the locus of Cenozoic continental breakup. The interpreted dataset images a ~6 km thick continental crust in which the Moho and the base of syn-rift sediment are observed as clear, well-resolved seismic reflections. This extremely thinned continental crust was offset at its base by a complex detachment fault system from which oceanward-dipping listric faults propagated vertically to bound six separate tilted blocks, in a style akin to tectonic rafts. The seismic reflection data in this work allowed us to investigate the thickness of syn- and post-rift strata above tilt blocks to reveal that the early-middle Eocene syn-rift topography was gradually blanketed in the late Eocene (~38 Ma). After 33 Ma (earliest Oligocene), the main depocenter on the margin migrated to the south of the Liwan Sub-basin, i.e. oceanward, as recorded by the thickening of strata within a *breakup sequence*. This work is important as it demonstrates how closely structures and sedimentation within the Liwan Sub-basin were controlled by a basal, rift-related detachment system, which is imaged in detail by 3D seismic data for the first time on a rifted continental margin. Continental breakup was marked by a shift in the locus of subsidence (and crustal stretching) toward ocean crust, within a time period spanning ~16 m.y. We extrapolate our findings from the South China Sea to the development of asymmetric passive margins across the world.

Keywords: Continental margins; South China Sea; Syn-rift; Continental breakup; Depth-dependent stretching; Structure; Depositional architecture.

1. Introduction

Stratigraphic and geophysical data on rifted margins have revealed complex relationships between continental rifting, continental breakup and seafloor spreading processes (Franke et al., 2014; Leroy et al., 2013; Peron-Pinvidic et al., 2013; Unternehr et al., 2010; Whitmarsh et al., 2001). In particular, information on rift-to-drift processes gathered from Atlantic margins (Boillot et al., 1987) have been complemented by outcrop data from the Mesozoic continental margins that bordered the ancient Tethys Ocean (Froitzheim and Eberli, 1990; Manatschal, 2004; Manatschal and Bernoulli, 1999; Mohn et al., 2010; Tugend et al., 2014). The evolution and geometry of these rifted margins is characterized by a set of comparable structural elements, namely distinct proximal, necking, distal, outer marginal highs and oceanic domains (Peron-Pinvidic et al., 2013).

Of particular scientific interest are the architecture and tectonic evolutions of the distal domain of rifted margins, as they record the transitional period between continental rifting and the onset of seafloor spreading (Alves and Abreu Cunha, 2018; Manatschal, 2004; Soares et al., 2012). Low-angle detachment faults in these distal domains have been shown to separate different crustal units during the exhumation of subcontinental mantle at the ocean-continent transition (OCT). These low-angle detachment faults are seemingly able to accommodate the bulk of crustal stretching during the last stages of continental rifting (de Charpal, 1978; Reston et al.,

1996), but are seldom identified on geophysical data due to sharp variations in their geometry, and the thick sediment cover accumulated above them (Krawczyk et al., 1996). Proof of these difficulties in identifying detachment faults solely based on seismic data has been the ongoing debate around the definition of a clear detachment offshore Galicia (S reflector; Hoffman and Reston, 1992; Reston et al., 1996) and further southward Iberia Abyssal Plain (H reflector; Krawczyk et al. 1996; Dean et al., 2008), based on vintage, relatively low-quality seismic data. This debate is often compounded by the presence of a relative thick sediment cover above hyperextended crust that lacks, on many a continental margin, stratigraphic constraints robust enough to characterize the tectonic events leading to continental breakup. Closer to the study area in this paper, hyper-extended crust has been observed above basal detachments on several seismic profiles from the northeast (McIntosh et al., 2014; Lei et al., 2018), north (Baiyun and Liwan Sub-basins) (Yang et al., 2018; Larsen et al., 2018; Sun et al., 2016), northwest (Xisha Trough) (Lei et al., 2016), and southwest (Nam Con Son Basin) (Savva et al., 2014) regions of the South China Sea. However, little is still known about spatial variations in these detachment faults, their 3D geometry and evolution.

In contrast to previous studies that used regional 2D seismic profiles with limited borehole stratigraphic constraints, this paper uses new high-quality 3D and 2D seismic data with significant recording lengths, 10 s two-way time (TWT), correlated with exploration wells that drilled into Paleogene syn-rift strata of a distal part of the South China Sea (Fig. 1). The interpreted 3D seismic volume, imaging the Liwan Sub-basin, addresses the relative lack of high-resolution seismic data on distal rifted margins (Fig. 1b). Here, we document the structural styles and crustal configurations during rifting and continental breakup of the distal part of the northern South China Sea. We focus our analysis on the tectonic-sedimentary records and fault geometries of the region just inboard from the locus of continental breakup (Figs. 1b, 2 and 3). The evolution of lithospheric thinning that leads to continental breakup has not been well defined in the literature, especially during the late phases of this process. Hence, this work is relevant to rifted margins across the world as it documents on a regional scale, for the first time, and using 3D seismic data of high quality:

a) the 3D geometries of a lower crust detachment fault system, of overlying tilt blocks, and associated syn-rift depocentres in the most distal part of a rifted margin;

b) that continental crust has been extremely thinned below the detachment fault system, a character suggesting that detachment faults form abrupt, tectonic boundaries during continental breakup;

c) that post-rift units were moderately faulted in the investigated region of the South China Sea when seafloor spreading was initiated.

2. Geological setting

The South China Sea is the largest marginal sea in the West Pacific region (Wang and Li, 2009) (Fig. 1a). After continental breakup, it recorded a relatively high ocean spreading rate approaching 2.5 cm/yr, half rate (Briais et al., 1993; Li et al., 2014; Larsen et al., 2018). These rates are comparable with what Searle (2013) classified as *intermediate seafloor spreading rates*. Drilling result from IODP Expeditions 367&368 shows initiation of Mid-Ocean Ridge basalt type magmatism during breakup, and a narrow and rapid transition from distal margin to the igneous oceanic crust (Larsen et al., 2018).

The South China Sea is divided into three NE–SW trending regions, i.e., the northern continental margin, the oceanic basin and the southern continental margin (Sibuet et al., 2016) (Fig. 1a). The northern margin of the South China Sea is >450 km wide and consists of a rifted continental shelf with broad deep-water basins (Fig. 1b). Continental rifting was first recorded in the late Cretaceous-early Paleocene and continued into the Oligocene (Ru and Pigott, 1986; Su et al., 1989; Clift et al., 2001). Before the late Cretaceous, the South China Sea was part of a continental arc generated by subduction of the Paleo-Pacific plate under SE Eurasia (Zhou et al., 2008; Taylor and

Hayes, 1980). Subsequent crustal extension, continental breakup and final separation between the northern and southern margins of the South China Sea started at ~30 Ma (early Oligocene), as first indicated by magnetic anomalies in its East Sub-basin (Briais et al., 1993; Taylor and Hayes, 1980). After this first continental breakup event, the oceanic spreading ridge jumped southward (Briais et al., 1993; Ding et al., 2018). Hsu et al (2004) argued that the oldest oceanic crust is late Eocene off South Taiwan. Recently, IODP Expedition 349 and deep-tow magnetic surveys investigated the East Sub-basin to estimate that seafloor spreading started there at ~33 Ma (earliest Oligocene), ceasing at ~15 Ma (Langhian; Li et al., 2014). The difference in ages for continental breakup between the East Sub-basin and the region off South Taiwan indicates that continental breakup propagated from east to west along the northern margin of the South China Sea (Franke et al., 2014; Sibuet et al., 2016).

The study area, the Liwan Sub-basin, is close to ODP Site 1148 (Wang et al., 2000) and IODP Site 349 (Li et al., 2015), along the northern margin of the South China Sea, in the distal part of the Pearl River Mouth Basin (Fig. 1b). The Pearl River Mouth Basin, with an area of 17.5×10^4 km^2, is the northernmost of a series of Cenozoic sedimentary basins developed along the northern margin of the South China Sea (Fig. 1b). The Pearl River Mouth Basin consists of a continental shelf and a broad deep-water continental slope (Fig. 1b). Based on the recognized age for the breakup unconformity (~33 Ma), the sediment infill in the Pearl River Mouth Basin and slope can be divided into two megasequences, namely the Eocene syn-rift supersequence (comprising the Wenchang and Enping Formations) and the Oligocene to Quaternary post-rift supersequence (with the Zhuhai, Zhujiang, Hanjiang, Yuehai and Wanshan Formations) (Fig. 2). Thus, we define the sequence boundary dated as ~33 Ma to be a breakup unconformity (T70 in Figure 2), bounding a *breakup sequence* at its base (Alves and Cunha, 2018; Soares et al., 2012; Zhao et al., 2016). The stratigraphic units and associated rifted structures below this *breakup sequence* are of primary interest to this study (Fig. 2).

High-resolution seismic data have shown that the Pearl River Mouth Basin was filled by large volumes of sediment delivered by the Pearl River from Oligocene to the Quaternary. The Pearl River has been the major drainage system in South China since, at least, the early Miocene (Clift et al., 2002). Before the onset of Oligocene continental breakup, the Pearl River Mouth Basin was filled by sediment derived from proximal continental sources; geochemistry data indicate the existence, at the time, of a restricted (regional) river basin, smaller than the modern Pearl River (Liu et al., 2017). Overlying the breakup unconformity, a *breakup sequence* sensu Soares et al. (2012) is characterized by the incision of submarine channel systems, significant mass-wasting, and widespread volcanism (Gong et al., 2013; Sun et al., 2017).

3. Data and methods

The distal part of the northern South China Sea was previously imaged and studied using 2D seismic-reflection surveys and regional geophysical methods (Gao et al., 2015; Lei et al., 2018; Lester et al., 2014; McIntosh et al., 2014; Zhu et al., 2012; Yang et al., 2018). In this study, new 3D and regional 2D data tied to borehole stratigraphic information, are used to examine the structural and tectono-stratigraphic evolutions of the deep-offshore Liwan Sub-basin (Figs. 1b and 1c). As the syn-rift evolution of the Liwan Sub-basin is still poorly understood - only shallow-penetration seismic profiles acquired during the 1990s have been interpreted in the region – the China National Offshore Oil Corporation (CNOOC) acquired a ~190 km-long deep-penetration seismic reflection profile (ZJK2012-1-2) using an airgun source, which recorded data to a depth of 10 s TWT and to provide much improved images of the Yunli High, Liwan Sub-basin and its oceanward region (Fig. 1b).

Previous studies have published part of the ZJK2012-1-2 seismic profiles using limited stratigraphic constraints on the syn-rift interval (Yang et al., 2018; Larsen et al., 2018; Sun et al.,

2016). Our study uses a new high-resolution 3D seismic volume (BLK4311), covering more than ~2000 km^2 of the Liwan Sub-basin, acquired in this decade. This volume was processed to a main frequency bandwidth of 30–45 Hz, with a Common Mid-Point (CMP) spacing of 12.5 m, and a recording length of 8.2 s TWT. The interpreted seismic volume provides an important opportunity to examine the 3D geometry of the syn-rift interval and its boundary faults over the entire extent of the Liwan Sub-basin, and at high resolution, something not achieved by the previously published 2D seismic profile ZJK2012-1-2 (Yang et al., 2018; Larsen et al., 2018).

All available academic and industrial wells were considered in this study. For this work, we chose wells that penetrate into Paleogene syn-rift strata (Fig. 1b). Well LW116 (water depth: 1495 m) was drilled on the Yunli High (Fig. 1c). Data from ODP Site 1148 (water depth: 3294 m; Wang et al., 2000) and IODP Site U1435 (water depth: 3252 m; Expedition 349 Scientists, 2014) were drilled along the southeastern edge of the Liwan Sub-basin (Fig. 1b).

The interpretation of 3D and 2D seismic data was based on the recognition of main sequence boundaries and associated seismic-stratigraphic sequences (Mitchum et al., 1977; Posamentier and Vail, 1988). Gamma-ray (GR) curves, resistivity (RT) logs, and stratigraphic data from Well LW116, helped the interpretation of seismic reflections and structures on Schlumberger's Geoframe® (Fig. 2). Absolute ages for regional stratigraphic horizons were based on stratigraphic data from wells provided by the CNOOC on the Yunli High (wells LW116 and LW114), and previous data acquired on the distal margin by ODP Site 1148 (Wang et al., 2000) (Fig. 1b).

4. Results

4.1 Upper crustal structure and detachment faulting on 2D seismic data

Located close to oceanic crust, seismic profile ZJK2012-1-2 images the Yunli High, the Liwan Sub-basin, and the southern edge of the Liwan Marginal High, as well as magnetic anomaly C11 (Fig. 3). The location of magnetic anomaly C11 was defined by Briais et al. (1993), who proposed an unequivocal oceanic crust at this same location.

In the 2D profile ZJK2012-1-2, Horizon Tg comprises a high-amplitude seismic reflection separating syn-rift strata from the pre-rift crystalline basement (Fig. 3). It forms a continuous horizon, except when intersected by large normal faults. Above Horizon Tg are observed thick Cenozoic strata with continuous reflections of variable amplitude (Fig. 3). A distinct reflection at ~9 s TWT is observed on the seismic profile in Fig. 3, at the same level one observes an increase in p-wave velocity (V_p) to >7.8 km/s on refraction data (Gao et al., 2015; Qiu et al., 2013). In the region of unequivocal oceanic crust, the Moho ascends from 9 s TWT in the Liwan Sub-basin and its marginal high, to 8 s TWT in oceanic crust, and continues at this depth toward the southeast edge of the 2D seismic profile (Fig. 3). Significantly, between the Moho and Horizon Tg there is a sub-horizontal reflection that is firstly imaged to extend from the Liwan Sub-basin to the Liwan Margin High. We labeled this feature the 'R' reflector on the seismic profile in Fig. 3. The 'R' reflector rises from ~8.5 s TWT approximately 65 km northwest of the seismic profile to ~6.5 s TWT about 140 km to the northwest (Fig. 3).

The crust overlying the 'R' reflects reveals a typical rift geometry comprising rotated tilted blocks bounded by south-dipping normal faults (blocks A, B and F; Fig. 3). These normal faults detach and sole out in a large listric fault, the Main Liwan Detachment (MLD; Fig. 3). Between the Yunli High and the Liwan Sub-basin, the MLD generated a break-away structure that dissected the continental blocks oceanward in the Liwan Sub-basin, and detaching on the 'R' reflector to the southeast of the profile in Fig. 3. The MLD is imaged as a high-amplitude wavy horizon and is deflected at ~6.5 s TWT under the Liwan Marginal High to the southeast (Fig. 3). However, at the transition zone between the Liwan Marginal High and oceanic crust, the MLD

and 'R' reflector are not observed (Fig. 3). Oceanward, except for several high-angle small faults offsetting unequivocal oceanic crust, no strong seismic reflections are found within the upper crust (Fig. 3).

4.2 Cenozoic strata above the Main Liwan Detachment (MLD)

Cenozoic strata in the Liwan Sub-basin reaches a maximum thickness of ~3.9 s TWT (~4.5 km) at a distance of ~40 km from the continental shelf, as shown by the regional 2D seismic profile in Fig. 3. It is important to stress that, below this sedimentary cover, the Moho reflector in profile ZJK2012-1-2 shallows gradually toward the south (i.e. oceanward). The thickness of the continental crust under the Yunli High, the Liwan Sub-basin, and the Liwan Marginal High is ~6.6 s TWT, ~1.9 s TWT and ~4.2 s TWT thick, respectively. Assuming an average velocity of 6.0 km s^{-1} for the continental crust (Xia et al., 2010), crustal thickness reaches, respectively, ~19.8 km, ~5.7 km, and ~12.6 km below the latter structural features.

To the southeast of the profile (i.e. oceanward), the Moho reflection is not a sharp boundary, rather forming a transitional zone between magnetic anomaly C11 and the most distal continental crust (Fig. 3). The Moho reflection occurs ~1.7-1.9 s TWT below the top of the oceanic basement, indicating a ~5.1-5.7 km thick oceanic crust at the location of anomaly C11. Oceanic crust thickness remains constant for tens of kilometers beyond this point (Fig. 3).

4.3 Borehole descriptions of syn-rift strata

Well LW116, located on the Yunli High (Fig. 1c), drilled continuously to a depth of 2318 meters below the sea floor (mbsf). It is also the only well in the study area that penetrated the crystalline basement; a gray black schist with a lepido granoblastic texture and schistose fabric. The age of this basement is likely > 56 Ma because it underlies the syn-rift Wenchang Formation, whose age ranges between 56 Ma and 38 Ma. The drilled section above Horizon T70 is similar to the lithofacies described at ODP Site 1148, which did not drill syn-rift strata.

Figure 2 shows syn-rift strata in Well LW116. The drilled section between 2244 mbsf and 2292 mbsf is correlated with the syn-rift Wenchang Formation based on biostratigraphic data acquired by exploration companies. The late syn-rift Enping Formation is absent in Well LW116 and very thin sediment was observed in the Liwan Sub-basin. Syn-rift strata in the Wenchang Formation, drilled by well LW116, is associated with two different sandstone lithofacies. The upper lithofacies between 2244 mbsf and 2262 mbsf consists of moderately sorted, fine-grained sandstones. The lower lithofacies at well LW116 (2262–2292 mbsf) comprises gray fine-grained to pebbly sandstones with sub-angular and semi-rounded quartz grains. Pebbly intervals in the sandstones are poorly sorted and with clasts 7~12 mm in diameter, the largest being ~20 mm. An interval composed of interbedded mudstones overlies the top of the sandstone unit in the upper lithofacies. The gamma-ray (GR) curve for the section drilled between 2262 mbsf and 2292 mbsf shows a bell-shaped pattern at this level (Fig. 2).

5. Hyperextended rift system imaged on 3D seismic data

5.1 Stratigraphic units and associated syn-rift fault systems

A key result from the interpretation of 3D seismic data was the division of basement rocks and Cenozoic deposits in the Liwan Sub-basin into six seismic units of regional expression (Figs. 2, 3 and 4). This division is based on their internal seismic character, data from ODP Site 1148, and information from exploration wells LW116 and LW114 (Figs. 1c and 2). From top to bottom, syn-rift strata are separated from post-rift units by the regional unconformity T70 (Figs. 2 and 3). Horizon T70 comprises a distinct unconformity of high amplitude that is markedly continuous, and of high amplitude, across the margin, as observed on the regional seismic profile in Fig. 3. Horizon T70 forms an angular unconformity near the

shoulder of the Liwan Sub-basin, but in its center changes to a concordant high-amplitude seismic reflection (see also Soares et al., 2012) (Fig. 3).

Horizon Tg is another prominent unconformity imaged on the interpreted seismic data; it forms an angular unconformity of regional expression separating pre-rift from syn-rift strata (Fig. 3). Horizon Tg is locally observed in the Liwan Sub-basin because it is offset by the MLD, which accommodates a heave of several kilometers (Fig. 3).

Seismic profile 630 crosses the eastern domain of the Liwan Sub-basin, imaging the MLD as a high-amplitude seismic reflection (Fig. 4). Overlying the basal detachment is a package of sediment offset by secondary faults that propagated from the MLD, among which faults F13, F15 and F16 are relatively large with several kilometers of displacement (Fig. 4). Faults F13, F15 and F16 are high-angle, south-dipping structures when crossing the sedimentary cover. At depth, they sole out in older Cenozoic sediments to merge with the MLD (Fig. 4).

A rotated tilt-block (Block C) is observed in the central part of the Liwan Sub-basin, towards the southern part of seismic profile 500 (Fig. 5). The MLD underlies Block C, whereas to the south of Block C is fault F16 (Fig. 5). On the top of Block C is a small graben bounded by a relatively small fault. Apart from fault F16, faults F11, F14 and F15 also offset the syn-rift stratigraphic intervals (Fig. 5). The style of these faults is similar to that shown in seismic profile 630, as they sole out at the MLD (Fig. 4). In the western part of the Liwan Sub-basin, similar geometries are observed above the MLD, with secondary faults bounding tilt-blocks A and B in seismic profile 370 (Fig. 6).

A second regional angular unconformity (T80), which is laterally continuous and of high amplitude, is observed in the succession bounded by Horizons Tg and T70 (Figs. 4, 5 and 6). Horizon T80 separates the syn-rift Wenchang Formation from the Enping Formation above (Figs. 4, 5 and 6). The Wenchang Formation, bounded by Horizons Tg and T80, is characterized by the presence of clinoforms reflecting a progradational trend, with marked downlap onto its lower boundary as one progresses oceanward (Fig. 5).

When compared to strata below, Horizon T70 is relatively continuous, showing variable amplitude across the 3D seismic survey (Figs. 4, 5 and 6). Faults deforming the Wenchang and Enping Formations can intersect Horizons T70 and even T60 locally, but most normal faulting ceased at the time of deposition of Horizon T40 in the central (Fig. 5) and western (Fig. 6) parts of the 3D seismic volume. The exception to this rule are the few small-offset faults observed at the level of Horizon T40 in the eastern part of the 3D seismic volume (Fig. 4). Small-scale faults are imaged in the upper part of the interval bounded by T60 and T40, and their character is similar to polygonal faults described in the North Sea (Lonergan et al., 1998).

A time-structural map for base Cenozoic strata is shown in Figure 7, revealing at the same time the present-day TWT depth of basement units. Except for the Yunli High, there are six structural highs in the study area that correlate with the tilted blocks observed in Figs. 4, 5 and 6. For example, in the southern central part of seismic profile 500 (Fig. 5), one structural high is imaged as a tilted continental block overlying the MLD, with a size of ~26.9 km^2.

We identified six tilted blocks with distinct sizes in the study area and named them Blocks A to F (Fig. 7 and Table 1). The largest of these tilted blocks, Block A, is located in the northern central part of seismic profile 370 (Fig. 6). Block A is bounded at its base by the MLD and to the south by fault F11. All the observed tilted blocks are bounded and isolated by secondary faults on their southern flanks, which sole out on the MLD (Fig. 4). The base of imaged tilted blocks thus coincide with the MLD or a secondary decoupling horizon, indicated they are extensional allochthons (see 2D seismic profile in Fig. 3).

5.2 Two-way time (TWT) attribute data

Attribute slices were extracted from the interpreted 3D seismic volume at a spacing of 50 ms (Fig. 1). Figure 8 shows the subsurface geologic map based on amplitude and coherence

slices at 4000 ms and 5400 ms. The coherence slice at 4000 ms images a linear feature that is associated with the boundary between Yunli High and the Liwan Sub-basin; it comprises the MLD fault. The deepest of time slices at 5400 ms images the MLD fault as a linear feature in the northern part of the 3D seismic volume. The MLD can be traced on the coherence slice in Figure 8b3 although the amplitude difference between the Yunli High and Liwan Sub-basin is not as marked here as its overlying coherence slice in Figure 8a3.

The strike of the MLD is locally variable, but its general trend is consistently to the east. Both time slices intersect the syn-rift succession in the central and southern domains of the Liwan Sub-basin, where the strike of seismic reflections is variable and multiple E-W features are imaged on successive coherence slices due to pervasive faulting (Fig. 8). On these same coherence slices, a set of east-trending normal faults (F11, F13, F14, F15 and F16) are also identified, and show lengths >15 km in map view. Between these large scale faults, a series of smaller east-trending faults are also imaged on the coherence data (Figs. 8a3 and 8b3). The northern part of the TWT slice at 5400 ms, and some of its central parts, are dominated by a reflection-free zone that is consistent with the presence of crystalline basement on the interpreted seismic profiles, e.g. the Yunli High, and Blocks A, C, D and F. Broad anticlinal structures overlie the basement (Figs. 4, 5 and 6).

The shallowest time slice at 4000 ms shows circular features in map view (Fig. 8a1). Dense small-scale, short length linear structures are also observed. These are consistent with the presence of small faults affecting the largest tilted blocks (Figs. 4, 5 and 6). In addition, high-amplitude and discontinuous reflections are observed to the north of the MLD (Fig. 8b1-b3), correlating with a set of discontinuous, high-amplitude seismic reflections on the footwall of the MLD (e.g. Fig. 4).

5.3 Sediment thickness in the Liwan Sub-basin

Figure 9 shows isopach maps for stratigraphic units described in the Liwan Sub-basin. At early-mid Eocene level (syn-rift), the thickness of the sediment is variable across the study area (Fig. 9a). The study area is characterized by relatively thin strata in the northern part of the survey, where they are directly deposited on the MLD (Fig. 4). The general trend of this thin interval of strata is east-west (Fig. 9a). Other areas with thin sediment are located on tilted blocks developed in the central and southern domains (Fig. 9a). Between distinct structural highs, several depocentres are observed (Fig. 9a). The largest thickness of early-mid Eocene strata is ~3000 m in the northern part of the 3D seismic volume, filling depocenters bounded by the Yunli High to the north and Block A to the south (Fig. 9a). Another east-striking depocenter occurs in the central domain, bounded by Block A to the north and Block B to the south. Other observed depocenters are north-striking (Fig. 9a).

In Figure 9b we observe that strata are relatively thin at upper Eocene level when compared with the lower Eocene. The largest thickness approaches ~750 m in the southeastern corner of the map. The variable thickness in Lower Eocene strata indicates important fault activity at this time, with faulting being significantly reduced during the late Eocene.

Overlying Horizon T70 is the post-rift interval, whose thickness is shown in Figure 9c. There are several distinct high-amplitude reflections within this post-rift interval, e.g Horizons T60 and T40. Locally they are offset by basement faults with throws of less than <0.2 s TWT. Sediment distribution at Oligocene and Neogene levels is much different above T70 when compared to its underlying strata. The largest thickness of sediment is mapped in the southern domain of the survey, where it reaches 2850 m (Fig. 9c). The thickness of post-rift strata in the northern and central domains is relatively small, with the largest depocenter being located between the Yunli High, Block A and Block D (Fig. 9c). Here, post-rift strata reach 1750 m in thickness.

Figure 9d presents the total thickness of Cenozoic strata, whose character is similar to the isopach map for the early-mid Eocene when

continental rifting was initiated. However, basin subsidence is less than that attributed to the early-mid Eocene syn-rift episode.

6. Discussion

6.1 Tectonic uplift inboard of the region of continental breakup

The Liwan Sub-basin is crossed by high-angle faults recognized in previous studies (Gao et al., 2015; Zhu et al., 2012). In recent studies, these faults were found to be controlled by a basal detachment fault (Yang et al., 2018; Larsen et al., 2018; Sun et al., 2016). However, the variable geometry of this detachment fault along its trend, and of the sedimentary units above it, are only constrained by one or two regional 2D seismic profiles. The new 3D seismic volume in this work shows that the most distal part of the Liwan Sub-basin is deformed by a detachment fault (MLD) effectively comprising a major tectonic boundary fault between the Liwan Sub-basin and the Yunli High (Figs. 3 and 8). The MLD extends southward into the crust of the Liwan Marginal High (Fig. 3). The fault also soles out at depth, approaching the horizontal in the basement units (lower crust). A series of tilted crustal blocks and a relatively thick sedimentary succession overlie the MLD (Figs. 3-6).

In the Liwan Sub-basin, tilted crustal blocks are associated with movement in the MLD, which generated accommodation space between them. However, the stacking patterns of the syn-rift Wenchang Formation were controlled by high-angle faults (Stages 1 and 2 in Fig. 10), preceeding the generation of the MLD and associated low-angle faults observed on the seismic data (Figs. 3-6). The syn-rift Wenchang Formation is predominantly formed of sandstones interbedded with variable amounts of gravel, a character associated with the predominance of local sources of sediment at this time.

In a second stage, fault segments with variable displacement propagated into the stratigraphic sequence, due to enhanced extension at the MLD, adding to a total heave of around ~30 km across the Liwan Sub-basin. This large-scale heave accommodated by the MLD generated multiple, highly-rotated crustal blocks and large amounts of accommodation space that was filled by the Enping Formation, whose thickness was closely controlled by the MLD (Fig. 3). Despite the fact that the Enping Formation is still intersected by syn-rift faults, strata in this unit are relatively thin, when compared with the syn-rift Wenchang Formation.

Prominent erosion recorded in the Liwan Sub-basin, and the absence of the Enping Formation in Well LW116, suggest important uplift on the distal margin during Stage 3 (Fig. 10). The time span represented by the Enping Formation is ~5 m.y. (between 38 and 33 Ma), a period of time preceding final continental breakup in the northeastern part of the South China Sea (Li et al., 2014), and is consistent with the main stage of flank uplift described on Atlantic-type continental margins (Stage 3 in Fig. 10) (Falvey, 1974). In stage 3, the crust is thinned by a detachment fault system, accompanying the oceanward migration of sequential brittle faulting towards the region of future oceanic spreading center. This process is consistent with previous results from numerical modeling (Ranero and Perez-Gussinye, 2010) and the Iberian example described by Peron-Pinvidic and Manatschal (2010) for the North Atlantic Ocean.

After Stage 3, seismic reflections in the Liwan Sub-basin became sub-parallel and show variable amplitude (Figs. 4-6), indicating that the Liwan Sub-basin became gradually stable but subsiding as a whole after Horizon T40 (Stages 4 and 5 in Fig. 10) (see Alves and Cunha, 2018).

6.2 Hyperextended rift systems and overlying post-rift faults

The Pearl River Mouth Basin, in which the study area is included, extends between the unstretched South China Block, which comprises a ~33 km-thick crust on average (Nissen et al., 1995), and the South China Sea with an average ~5 km-thick oceanic crust (Fig. 3). The deep-penetration 2D seismic data constrained by the new 3D seismic volume and borehole data reveals a clear Moho reflection at ~9 s TWT below the

Liwan Sub-basin, pointing out to a minimum crustal thickness of ~6 km in this region (Fig. 3). Assuming that the present-day unstretched crust under Southern China can be a rough estimate for the initial crustal thickness in the South China Sea, we can determine a stretching factor β (McKenzie, 1978) for the study area. The crust on the distal margin reaches a minimum thickness of ~6 km, where we estimate a maximum β of ~4.5. Data from rifted basins worldwide indicate that stretching factors on the proximal margin are <1.5 (Davis and Kusznir, 2002). Comparatively, the estimated stretching factor β in the Liwan Sub-basin is much larger than on the proximal margin, confirming that the crust was extremely thinned.

Strikingly, crust gradually becomes thicker in a seaward direction from the Liwan Sub-Basin toward the distal margin, where a structural high, the Liwan Marginal High, reveals a near uniform thickness of ~12.6 km (Fig. 3). Our calculated β values for the Liwan Marginal High depend on the nature of the HVLC (high-velocity of lower crust), a characteristic body underlying the crust in and nearby the Liwan Sub-basin (Yan et al., 2001; Wang et al., 2006; Wei et al., 2011). If the HVLC represents magmatic material intruded into the lower crust, what one observes on seismic data represents the very final crustal thickness after rifting, and $\beta = \sim 2.5$ on the Liwan Marginal High. However, if the ~3-5 km-thick HVLC reflects the presence of underplated magmatic material at the base of the crust (Yan et al., 2001), the true thickness of the rifted continental crust may be ~9.6–7.6 km and $\beta = \sim 3.3–4.2$. Such an extreme crustal thinning would have led to continental breakup (Lester et al., 2014; Perez-Gussinye and Reston, 2001), and is responsible for the marked lateral translation of tilted crustal blocks above the MLD; a style akin to tectonic rafts. However, our data did not image precisely when, during the Cenozoic, the HVLC was formed on the northern margin of the South China Sea.

If continental breakup is only generated by crustal-scale faulting, one would observe the MLD to the north (landward) of unequivocal oceanic crust and offsetting this latter. However, the MLD truncates the 'R' reflector, the upper limit of lower crust flow (Fig. 3). A set of high-amplitude, sub-horizontal reflections observed in the volume of crust bounded by the 'R' reflector and the Moho confirms that a weak, low-viscosity zone in the lower crust exists between upper crust rocks and the Moho, as suggested for other margins (e.g. Abdelmalak et al., 2017; Clerc et al., 2015; Reston, 1988). On the northern margin of the South China Sea, depth-dependent extension modeled by Davis and Kusznir (2002), Clift et al.(2002) and Lei et al. (2016) indicate there is a flowing lower crust in this region. Thus, in contrast to previous interpretations, our data provide evidence for highly extended continental crust on the distal margin, where a low-angle detachment fault (MLD) soles out in the 'R' reflector at a depth of ~10-15 km. Our interpretation favors a setting in which the MLD and other basin-bounding normal faults offset the upper crust and merge with the ‘R’ reflector near the brittle-ductile transition. The MLD marks the lower boundary of brittle crustal deformation.

Although the normal faults propagating in the upper crust did create large basement offsets, at present they do not obviously offset the Moho to extend into the mantle (Fig. 3), contrasting with the observations in Hays et al. (1995). The 3D Seismic data in this work suggest that faulting is not the primary form of strain accommodation in continental crust. In contrast, strain is mainly accommodated in the thinned ductile lower crust. Clift et al. (2002) indicated the ductile crust below deep-water basins of the northern margin of the South China Sea was weak during active extension (Stages 3 and 4 in Fig. 10). However this mechanism, associated with pure shear, requires the formation of symmetric structures both on the northern and southern margins of the South China Sea. The data in this wok shows the South China Sea to be an asymmetric continental margin, and that detachment faulting played an important role during continental breakup, except for its lower crust. Such a setting can be explained by the formation of a shear zone beneath the brittle crust (Wernicke, 1995).

Detachment-fault models proposed to explain the crustal geometries on distal continental margins imply that extension is not

uniformly accommodated with depth, and that greater thinning of the lower crust occurs compared to the upper brittle crust (Davis and Kusznir, 2004; Driscoll and Karner, 1999). In contrast to the conceptual models underpinned by numerical modeling and constrained by geological and geophysical observation from the Alpine Tethys and Iberia-Newfoundland (Lavier and Manatschal, 2006), the Liwan Sub-basin in the South China Sea shows prolonged faulting after the onset of continental breakup, continuing at least until ~16.5 Ma (Stage 5 in Fig. 10) – an age consistent with cessation of oceanic spreading in the southern part of the South China Sea (Li et al., 2014). Thus, strata between Horizons T70 and T40 were deposited in a period of normal-fault activity that occurred after continental breakup to the northeast of the study area, and putatively form a *breakup sequence* sensu Soares et al. (2012) spanning the Oligocene-Early Miocene. Below Horizon T70, strata are affected by older faults that propagated vertically from the MLD, reflecting extreme crustal thinning. In this study, we suggest that prolonged faulting in the Liwan Sub-basin is typical of *intermediate ocean spreading* rates (Searle, 2013). Conversely, on continental margins around the Northern Atlantic Ocean, with slow spreading rates, minor faulting is observed in post-rift strata and the continental margin subsides as a whole during the continental breakup event (Sibuet and Tucholke, 2013; Alves and Cunha, 2018).

7. Conclusions

The largest 3D seismic volume this far acquired on a continental margin is interpreted here to reveal main crustal-scale structures on the most distal parts of the northern South China Sea. Together with a deep-penetration seismic profile tied to industry well data, the interpreted volume imaged highly extended crust, only ~6 km thick, on the distal margin of the northern South China Sea, just inboard of the locus of continental breakup.

The 3D seismic data also provided, for the South China Sea, first evidence for low-angle detachment faults that sole out at weak lower crust. Over a main detachment fault (MLD), six tilted blocks were translated at least ~5 km away from the Yunli High. Extension along the detachment fault generated large amounts of accommodation space for sediment, a result of the rotation of tilt blocks and their lateral translation (heave) in a style akin to tectonic rafts. During the early-mid Eocene syn-rift, proximal sources fed poorly sorted sediment to the Liwan Sub-basin. Subsequently, extensional faulting in the Liwan Sub-basin decreased in importance – but was still relatively active - during the late Oligocene, contrasting with the regional-scale subsidence observed in magma-poor margins. A *breakup sequence* spanning the Oligocene-Early Miocene represents this last stage of rifting and continental breakup.

Post-rift faults formed in the Oligocene and early Miocene are thus distinct from those observed in 'typical' magma-poor Atlantic margins. We suggest these younger faults to result from relatively faster oceanic spreading in the northern South China Sea, when compared to the slower spreading of magma-poor margins. This character reveals important fault-controlled subsidence during and immediately after continental breakup in *intermediate*, and putatively, *fast* ocean spreading margins.

Acknowledgements

This work was funded by Natural Science Foundation of China (No. 41830537), National Programme on Global Change and Air-Sea Interaction (GASI-GEOGE-02), Natural Science Foundation of China (No. 41772093), National Science and Technology Major Project of the Ministry of Science and Technology of China (2016ZX005008-001-001). National key research and development project (2017YFC1405502). We thank CNOOC, Beijing and Shenzhen for making their data available and in particular Weilin Zhu and Hesheng Shi for their valuable help. We also thank Dr. Gwenn Peron-Pinvidic, Dr. Christopher Jackson and Dr. Dieter Franke for commenting on an earlier version of this paper.

References:

Alves, T. M., and Abreu Cunha, T., 2018, A phase of transient subsidence, sediment bypass and deposition of regressive–transgressive cycles during the breakup of Iberia and Newfoundland: Earth and Planetary Science Letters, v. 484, p. 168-183.

Abdelmalak, M. M., Faleide, J. I., Planke, S., Gernigon, L., Zastrozhnov, D., and G. E. Shephard, A. R. M., 2017, The T-Reflection and the Deep Crustal Structure of the Vøring Margin, Offshore mid-Norway: Tectonics, no. 36, p. 2497-2523.

Boillot, G., Winterer, E. L., and Meyer, A. W., 1987, Leg 103: Proceeding ODP Initial Reports, v. 103, p. 663.

Briais, A., Patriat, P., and Tapponnier, P., 1993, Updated Interpretation of Magnetic Anomalies and Seafloor Spreading Stages in the South China Sea: Implications for the Tertiary Tectonics of Southeast Asia: Journal of Geophysical Research, v. 98, no. B4, p. 6299-6328.

Briais, A., Patriat, P., and Tapponnier, P., 1993, Updated Interpretation of Magnetic Anomalies and Seafloor Spreading Stages in the South China Sea: Implications for the Tertiary Tectonics of Southeast Asia: Journal of Geophysical Research, v. 98, no. B4, p. 6299-6328.

Clift, P., Lin, J., and Barckhausen, U., 2002, Evidence of low flexural rigidity and low viscosity lower continental crust during continental break-up in the South China Sea: Marine and Petroleum Geology, v. 19, no. 8, p. 951-970. Clift, P., and Lin, J., 2001, Preferential mantle lithospheric extension under the South China

margin: Marine and Petroleum Geology, v. 18, no. 8, p. 929-945.
Clerc, C., Jolivet, L., and Ringenbach, J., 2015, Ductile extensional shear zones in the lower crust of a passive margin: Earth and Planetary Science Letters, v. 431, p. 1-7.Davis, M., and Kusznir, N. J., 2004, Depth-dependent lithospheric stretching at rifted continental margins, *in* Karner, G. D., Taylor, B., Driscoll, N., and Kohlstedt, C., eds., Rheology and Deformation of the Lithosphere at Continental Margins, Columbia University Press, p. 92-136.
Davis, M., and Kusznir, N. J., 2004, Depth-dependent lithospheric stretching at rifted continental margins, *in* Karner, G. D., Taylor, B., Driscoll, N., and Kohlstedt, C., eds., Rheology and Deformation of the Lithosphere at Continental Margins, Columbia University Press, p. 92-136.
de Charpal, O., 1978, Rifting, crustal attenuation and subsidence in the Bay of Biscay: Nature, v. 275, p. 706-711.
Dean, S. M., Minshull, T. A., and Whitmarsh, R. B., 2008, Seismic constraints on the three-dimensional geometry of low-angle intracrustal reflectors in the Southern Iberia Abyssal Plain: Geophyscial Journal International, v. 175, no. 2, p. 571-586.
Ding, W., Sun, Z., Dadd, K., Fang, Y., and Li, J., 2018, Structures within the oceanic crust of the central South China Sea basin and their implications for oceanic accretionary processes: Earth and Planetary Science Letters, v. 488, p. 115-125.
Driscoll, N. W., and Karner, G. D., 1999, Lower crustal extension across the Northern Carnarvon basin, Australia: Evidence for an eastward dipping detachment: Journal of Geophysical Research, v. 103, p. 4975–4991.
Falvey, 1974, The development of continental margins in plate tectonic theory: J. Aust. Pet. Explor. Assoc., v. 14, p. 95-106.
Franke, D., Savva, D., Pubellier, M., Steuer, S., Mouly, B., Auxietre, J., Meresse, F., and Chamot-Rooke, N., 2014, The final rifting evolution in the South China Sea: Marine and Petroleum Geology, v. 58, p. 704-720.
Froitzheim, N., and Eberli, G. P., 1990, Extensional, detachment faulting in the evolution of a Tethys passive continental margin, eastern Alps, Switzerland, v. 102, no. 9, p. 1297-1308.
Gao, J., Wu, S., McIntosh, K., Mi, L., Yao, B., Chen, Z., and Jia, L., 2015, The continent–ocean transition at the mid-northern margin of the South China Sea: Tectonophysics, no. 654, p. 1-19.
Hayes, D. E., Nissen, S. S., Buhl, P., Diebold, J., Bochu, Y., Zeng, W., and Chen, Y., 1995, Throughgoing crustal faults along the northern margin of the South China Sea and their role in crustal extension: Journal of Geophysical Research Solid Earth, v. 100, no. B11, p. 22435-22446.
Hoffmann, H. J., and Reston, T. J., 1992, Nature of the S reflector beneath the Galicia Banks rifted margin: Preliminary results from prestack depth migration: Geology, v. 20, no. 12, p. 1091-1094.
Krawczyk, C. M., Reston, T. J., Beslier, M. O., and Boillot, G., 1996, Evidence for Detachment Tectonics on the Iberia Abyssal Plain Rifted Margin, *in* Whitmarsh, R., Sawyer, D., and Klaus, A., eds., Proceedings of the Ocean Drilling Program, Science Results: College Station, Tex., Ocean Drill. Program, p. 603-615.
Lavier, L. L., and Manatschal, G., 2006, A mechanism to thin the continental lithosphere at magma-poor margins: Nature, v. 440, no. 7082, p. 324-328.
Lei, C., Ren, J., Pang, X., Chao, P., and Han, X., 2018, Continental rifting and sediment infill in the distal part of the northern South China Sea in the Western Pacific region: Challenge on the present-day models for the passive margins: Marine and Petroleum Geology, v. 93, p. 166-181.
Lei, C., and Ren, J., 2016, Hyper-extended rift systems in the Xisha Trough: implications for extreme crustal thinning ahead of a propagating ocean of the South China Sea: Marine and Petroleum Geology, v. 77, p. 846-864.
Leroy, S., Razin, P., Autin, J., Bache, F., D Acremont, E., Watremez, L., Robinet, J., Baurion, C., Denèle, Y., and Bellahsen, N., 2013, From rifting to oceanic spreading in the Gulf of Aden: a synthesis, Lithosphere Dynamics and Sedimentary Basins: The Arabian Plate and Analogues, Springer, p. 385-427.
Lester, R., Van Avendonk, H. J., McIntosh, K., Lavier, L., Liu, C. S., Wang, T. K., and Wu, F., 2014, Rifting and magmatism in the northeastern South China Sea from wide- angle tomography and seismic reflection imaging: Journal of Geophysical Research: Solid Earth, v. 119, no. 3, p. 2305-2323.
Li, C. F., Lin, J., Kulhanek, D. K., and Scientists, T. E., 2015, Proceedings of the International Ocean Discovery Program Volume 349, International Ocean Discovery Program.
Li, C., Xu, X., Lin, J., Sun, Z., Zhu, J., Yao, Y., Zhao, X., Liu, Q., Kulhanek, D. K., and Wang, J., 2014, Ages and magnetic structures of the South China Sea constrained by deep tow magnetic surveys and IODP Expedition 349: Geochemistry, Geophysics, Geosystems, v. 15, p. 4958-4983.Liu, C., Clift, P. D., Carter, A., Böning, P., Hu, Z., Sun, Z., and Pahnke, K., 2017, Controls on modern erosion and the development of the Pearl River drainage in the late Paleogene: Marine Geology, v. 394, p. 52-68.
Lonergan, L., Cartwright, J., and Jolly, R., 1998, The geometry of polygonal fault systems in Tertiary mudrocks of the North Sea: Journal of Structural Geology, v. 20, no. 5, p. 529-548.
Manatschal, G., 2004, New models for evolution of magma-poor rifted margins based on a review of data and concepts from West Iberia and the Alps: International Journal of Earth Sciences, v. 93, no. 3, p. 432-466.
Manatschal, G., and Bernoulli, D., 1999, Architecture and tectonic evolution of nonvolcanic margins: Present-day Galicia and ancient Adria: TECTONICS, v. 18, no. 6, p. 1099-1119.
McKenzie, D., 1978, Some remarks on the development of sedimentary basins: Earth and Planetary Science Letters, v. 40, no. 1, p. 25-32.
Mitchum, R. M. J., Vail, P. R., and Sangree, J. B., 1977, Seismic stratigraphy and global changes of sea-level, part 6: stratigraphic interpretation of seismic reflection patterns in depositional sequences: Geophysical Research Letters, v. 29, no. 22, p. 7-1–7-4.
Mohn, G., Manatschal, G., Müntener, O., Beltrando, M., and Masini, E., 2010, Unravelling the interaction between tectonic and sedimentary processes during lithospheric thinning in the Alpine Tethys margins: International Journal of Earth Sciences, v. 99, no. 1, p. 75-101.
Nissen, S. S., Hayes, D. E., Buhl, P., Diebold, J., Bochu, Y., Weijun, Z., and Yongqin, C., 1995, Deep penetration seismic soundings across the northern margin of the South China Sea: Journal of Geophysical Research, v. 100, no. B11, p. 22407-22,433.
Perez-Gussinye, M., and Reston, T. J., 2001, Rheological evolution during extension at nonvolcanic rifted margins: Onset of serpentinization and development of detachments leading to continental breakup: Journal of Geophysical Research-Solid Earth, v. 106, no. B3, p. 3961-3975.
Peron-Pinvidic, G., Manatschal, G., and Osmundsen, P. T., 2013, Structural comparison of archetypal Atlantic rifted margins: a review of observations and concepts: Marine and Petroleum Geology, v. 43, p. 21-47.
Peron-Pinvidic, G., and Manatschal, G., 2010, From microcontinents to extensional allochthons: witnesses of how continents rift and break apart? Petroleum Geoscience, v. 16, no. 3, p. 189-197.
Posamentier, H. W., and Vail, P. R., 1988, Sequence Stratigraphy: Sequences and Systems Tract Development, *in* James, D. P., and Leckie, D. A., eds., Sequences, Stratigraphy, Sedimentology: Surface and Subsurface, Memoir 15, p. 571–572.
Qiu, N., Wang, Z., Xie, H., Sun, Z., Wang, Z., Sun, Z., and Zhou, D., 2013, Geophysical investigations of crust-scale structural model of the Qiongdongnan Basin, Northern South China Sea: Marine Geophysical Researches, v. 34, no. 3-4, p. 259-279.
Ranero, C. R., and Perez-Gussinye, M., 2010, Sequential faulting explains the asymmetry and extension discrepancy of conjugate margins: Nature, v. 468, no. 7321, p. 294-299.
Reston, T. J., Krawczyk, C. M., and Klaeschen, D., 1996, The S reflector west of Galicia (Spain): Evidence from prestack depth migration for detachment faulting during continental breakup: Journal of Geophysical Research-Solid Earth, v. 101, no. B4, p. 8075-8091.
Reston, T. J., Pennell, J., Stubenrauch, A., Walker, I., and Perez-Gussinye, M., 2001, Detachment faulting, mantle serpentinization, and serpentinite- mud volcanism beneath the Porcupine Basin, southwest of Ireland: Geology, v. 29, no. 7, p. 587.
Reston, T. J., 1988, Evidence for shear zones in the lower crust offshore Britain: Tectonics, v. 7, no. 5, p. 929-945.
Ru, K., and Pigott, J. D., 1986, Episodic rifting and subsidence in the South China Sea: AAPG Bulletin, v. 70, no. 9, p. 1136-1155.
Sibuet, J., and Tucholke, B. E., 2013, The geodynamic province of transitional lithosphere adjacent to magma-poor continental margins: Geological Society, London, Special Publications, v. 369, no. 1, p. 429-452.
Su, D., White, N., and McKenzie, D., 1989, Extension and subsidence of the Pearl River mouth basin, northern South China Sea: Basin Research, v. 2, no. 4, p. 205-222.
Sun, Z., Stock, J., Jian, Z., McIntosh, K., Alvarez-Zarikian, C. A., and Klaus, A., 2016, Expedition 367/368 Scientific Prospectus: South China Sea Rifted Margin, International Ocean Discovery Program. http://dx.doi.org/10.14379/iodp.sp.367368.2016.
Searle, R., 2013, Mid-Ocean Ridges, Cambridge University Press.
Taylor, B., and Hayes, D. E., 1980, The tectonic evolution of the South China Basin, in Hayes, D. E., ed., The Tectonic and Geologic Evolution of Southeast Asian Seas and Islands: Geophysical Monograph, American Geophysical Union, p. 89–104.
Tugend, J., Manatschal, G., Kusznir, N. J., and Masini, E., 2014, Characterizing and identifying structural domains at rifted continental margins: application to the Bay of Biscay margins and its Western Pyrenean fossil remnants: Geological Society, London, Special Publications, v. 413, p. SP413. 3.
Unternehr, P., Péron-Pinvidic, G., Manatschal, G., and Sutra, E., 2010, Hyper-extended crust in the South Atlantic: in search of a model: Petroleum Geoscience, v. 16, no. 3, p. 207-215.
Wang, P., and Li, Q., 2009, The South China Sea-Plaleoceanography and Sedimentology, Springer. Soares, D. M., Alves, T. M., and Terrinha, P., 2012, The breakup sequence and associated lithospheric breakup surface: Their significance in the context of rifted continental margins (West Iberia and Newfoundland margins, North Atlantic): Earth and Planetary Science Letters, v. 355-356, p. 311 - 326.
Wang, P., Prell, W. L., Blum, P., and Party, S. S., 2000, Proceedings of Ocean Drilling Program, Initial Report, Vol. 184: Ocean Drill. Program.
Wang, T. K., Chen, M. K., Lee, C. S., and Xia, K., 2006, Seismic imaging of the transitional crust across the northeastern margin of the South China Sea: Tectonophysics, v. 412, no. 3-4, p. 237-254.
Wei, X. D., Ruan, A. G., Zhao, M. H., Qiu, X. L., Li, J. B., Zhu, J. J., Wu, Z. L., and Ding, W. W., 2011, A Wide- Angle Obs Profile Across the Dongsha Uplift and Chaoshan Depression in the Mid- Northern South China Sea: Chinese Journal of Geophysics, v. 54, no. 6, p. 1149-1160.
Wernicke, B., 1995, Low-angle normal faults and seismicity: A review: Journal of Geophysical Research: Solid Earth, v. 100, no. B10, p. 20159-20174.
Whitmarsh, R. B., Manatschal, G., and Minshull, T. A., 2001, Evolution of magma-poor continental margins from rifting to seafloor spreading: Nature, v. 413, no.

6852, p. 150-154.
Xia, S., Zhao, M., Qiu, X., Xu, H., and Shi, X., 2010, Crustal structure in an onshore-offshore transitional zone near Hong Kong, northern South China Sea: Journal of Asian Earth Sciences, v. 37, no. 5-6, p. 460-472.
Yan, P., Di, Z., and Zhaoshu, L., 2001, A crustal structure profile across the northern continental margin of the South China Sea: Tectonophysics, v. 338, no. 1, p. 1-21.
Yang, L., Ren, J., McIntosh, K., Pang, X., Chao, L., and Zhao, Y., 2018, The structure and evolution of deepwater basins in the distal margin of the northern South China Sea and their implications for the formation of the continental margin: Marine and Petroleum Geology.
Zhou, D., Sun, Z., Chen, H., Xu, H., Wang, W., Pang, X., Cai, D., and Hu, D., 2008, Mesozoic paleogeography and tectonic evolution of South China Sea and adjacent areas in the context of Tethyan and Paleo Pacific interconnections: Island Arc, v. 17, no. 2, p. 186-207.
Zhu, J., Qiu, X., Kopp, H., Xu, H., Sun, Z., Ruan, A., Sun, J., and Wei, X., 2012, Shallow anatomy of a continent-ocean transition zone in the northern South China Sea from multichannel seismic data: TECTONOPHYSICS, v. 554, p. 18-29.

Figures

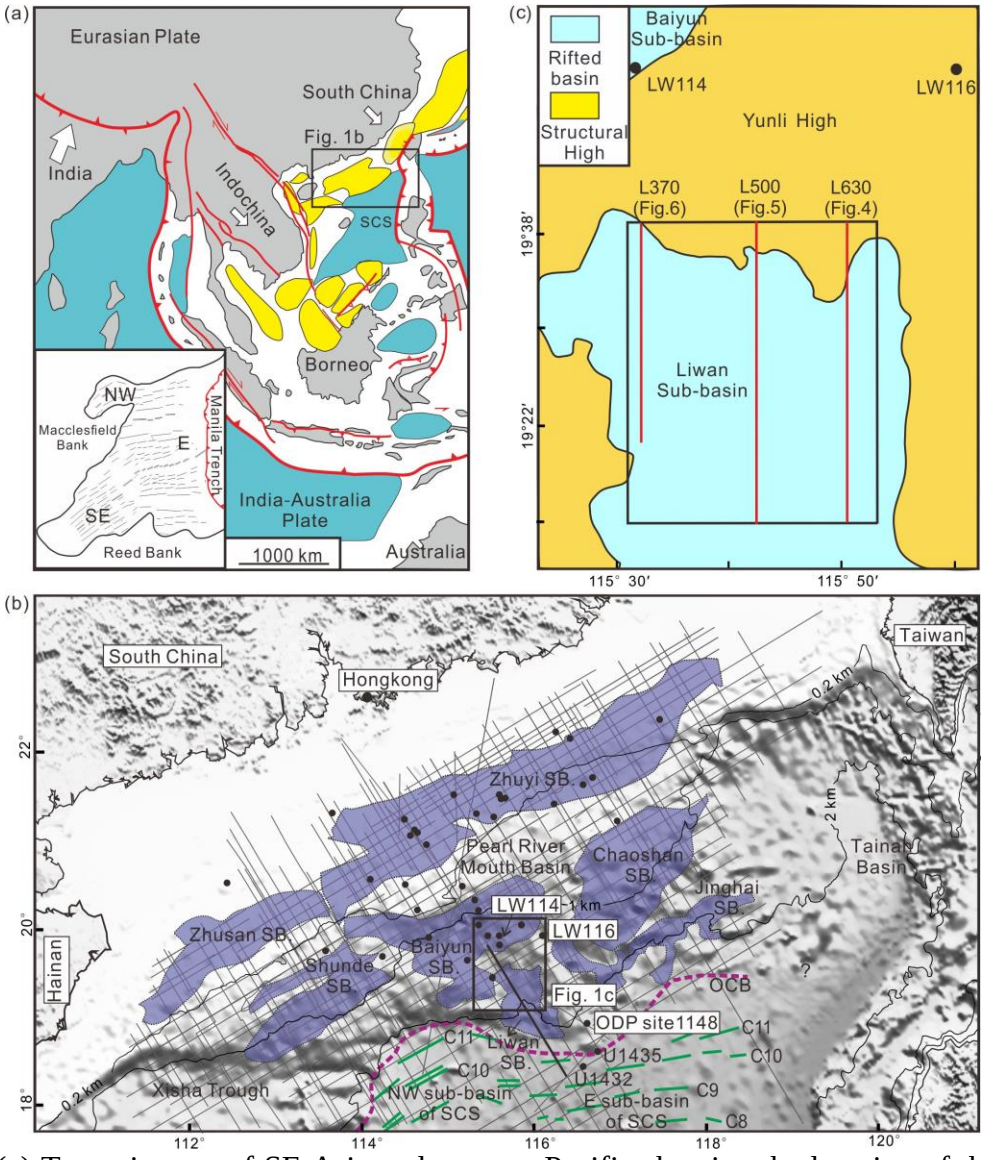

Figure 1. (a) Tectonic map of SE Asia and western Pacific showing the location of the northern margin of the South China Sea. Inset map shows the magnetic lineations in the South China Sea (Briais et al., 1993), which consists of NW, E and SW oceanic Sub- basins. (b) Location of the Pearl River Mouth Basin and associated sub-basins on the northern South China Sea. The Liwan Sub-basin is highlighted by the black box, where the 3D seismic volume BLK4311 was acquired. Available exploration wells and 2D seismic profiles are indicated by the black solid circles and gray lines, respectively. Note that the black solid line shows the location of the 2D deep-penetration seismic profile ZJK2012-1-2. The purple dash line and green solid lines show the continent-ocean boundary (COB) and magnetic lineations, respectively. The blue solid areas indicate the sub-basins in the Pearl River Mouth. SCS: South China Sea; SB: Sub-basin. (c) General structure of the Liwan Sub-basin and location of the 3D seismic data BLK4311. The seismic profiles interpreted in this work are indicated by the red solid lines.

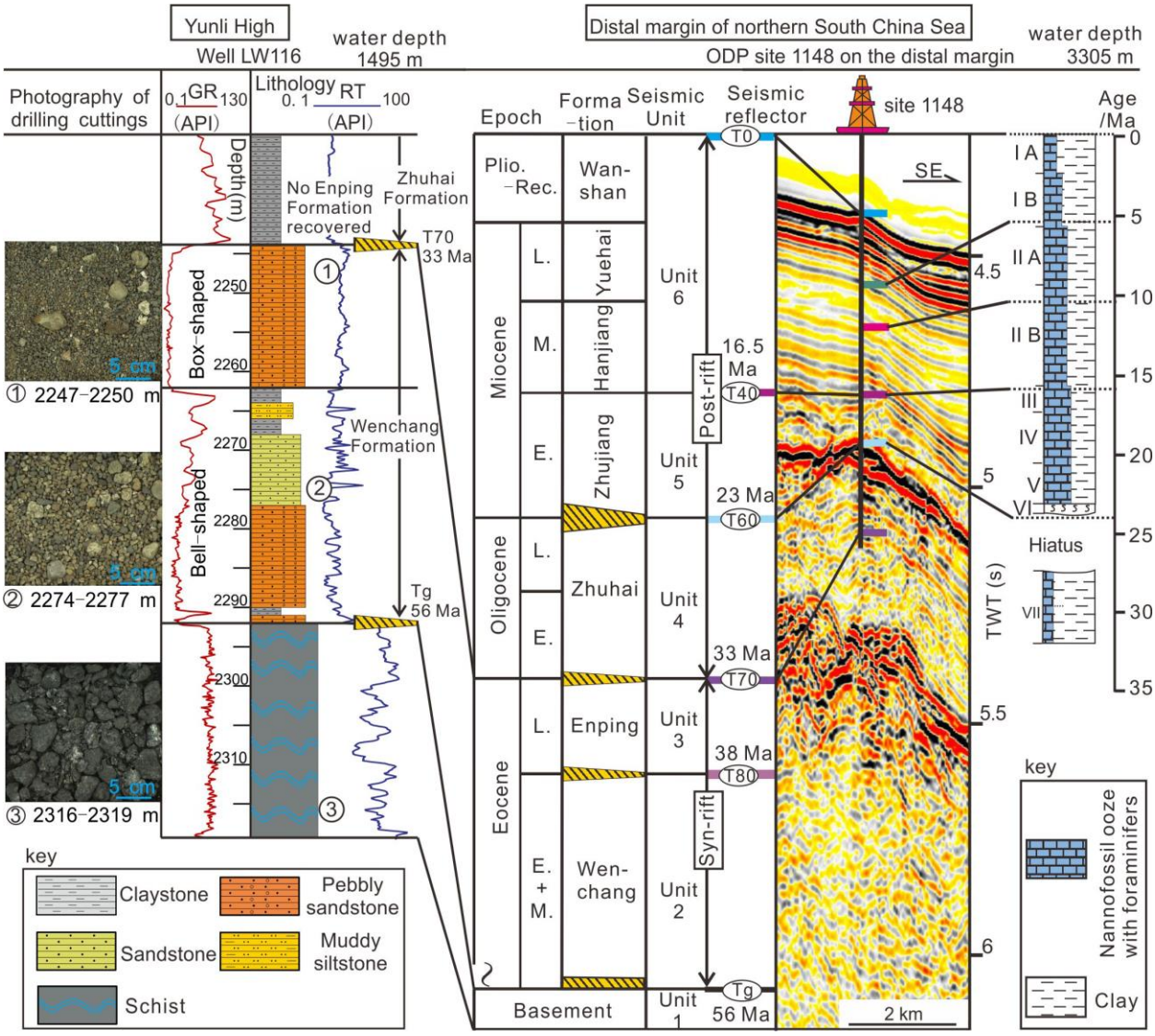

Figure 2. Stratigraphic and lithological data from exploration Well LW116 and for ODP Site 1148, as interpreted in this work. The stratigraphic data are correlated with the regional Cenozoic stratigraphy for the Pearl River Mouth Basin.

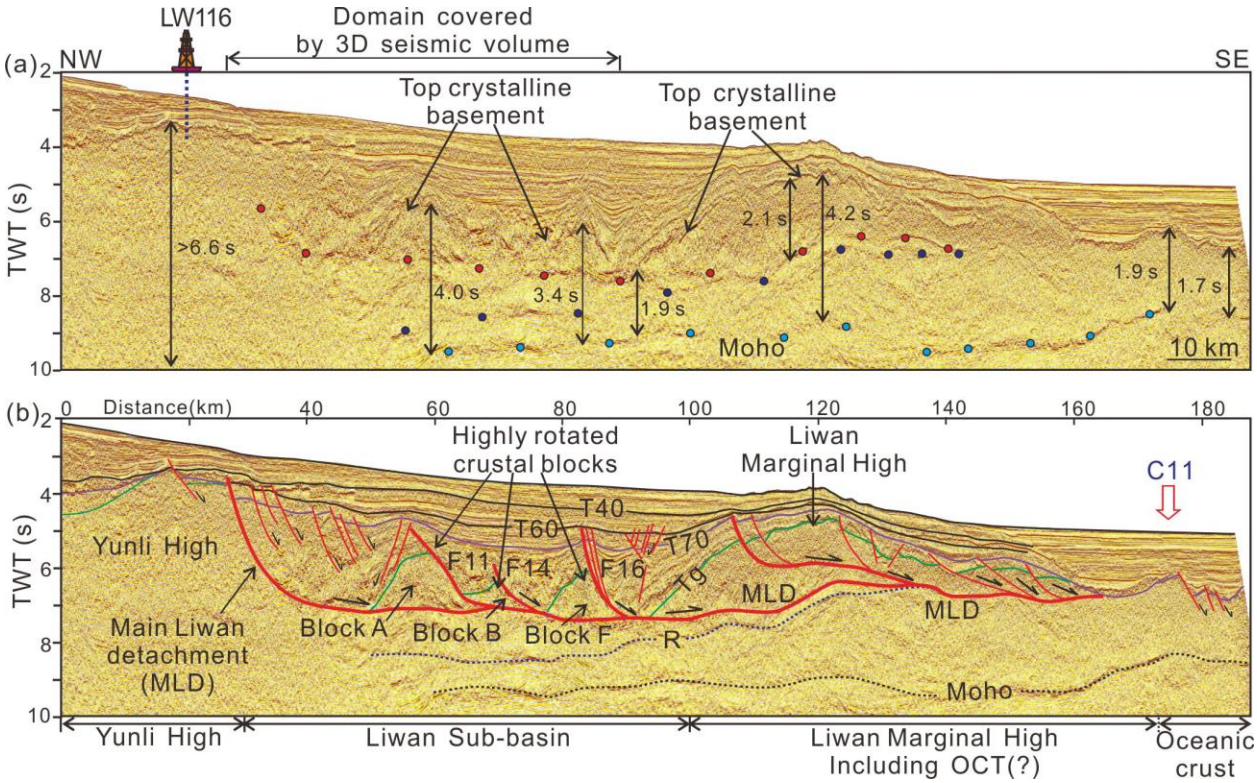

Figure 3. (a) Uninterpreted and (b) Interpreted seismic-reflection profile ZJK2012-1-2 across the Liwan Sub-basin and unequivocal oceanic crust (location shown in Fig. 1b). The interpreted profile shows the MLD and the general configuration of the upper crust, with half-grabens and tilted blocks. Exploration Well LW116 on the profile is projected – the well is located to the northeastern edge of the Liwan Sub-basin. The red, blue and green dots indicate main seismic reflections below extended crust. C11: magnetic anomaly C11. MLD: main Liwan detachment fault.

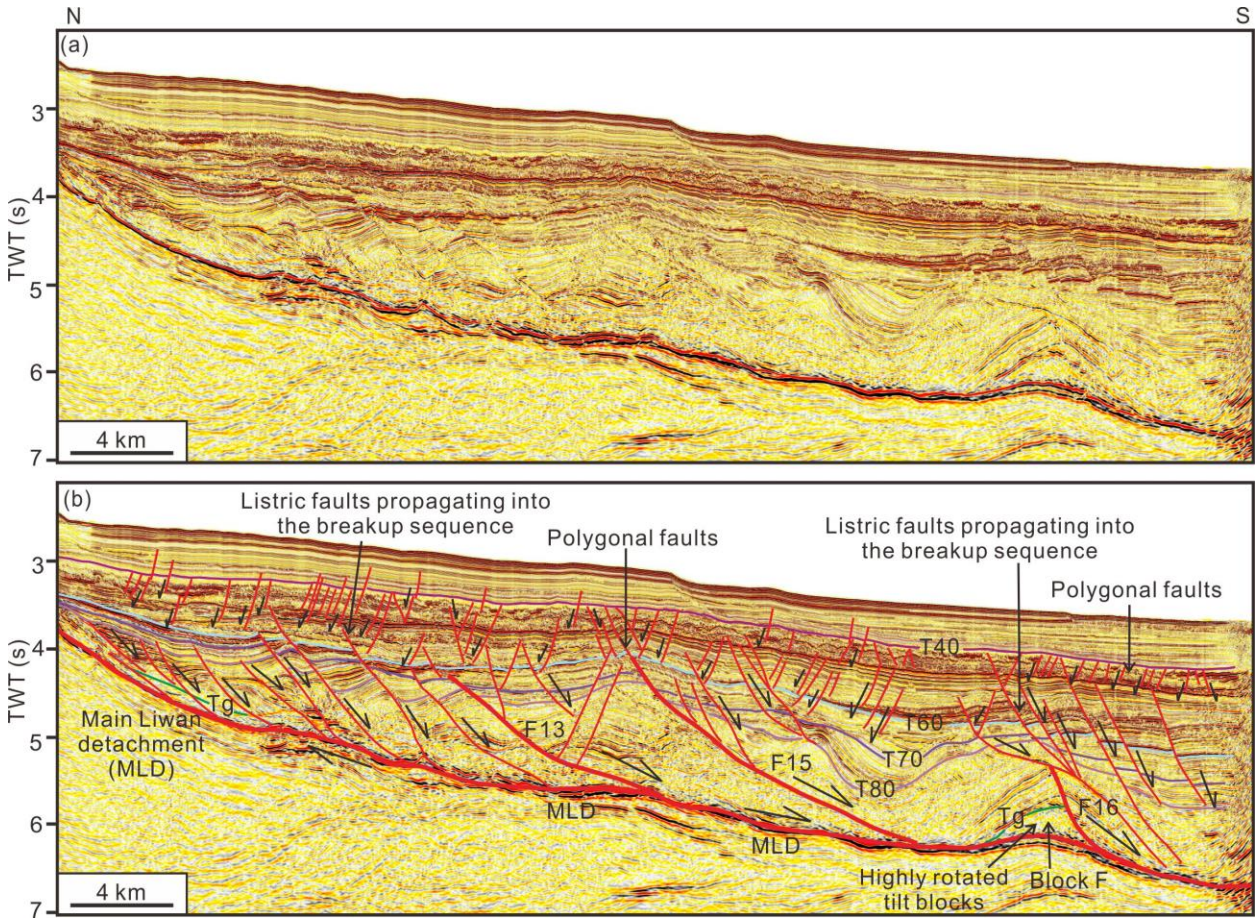

Figure 4. (a) Uninterpreted and (b) Interpreted north-south profile 630 from the eastern part of the 3D seismic volume. Location of the seismic profile is shown in Figure 1c.

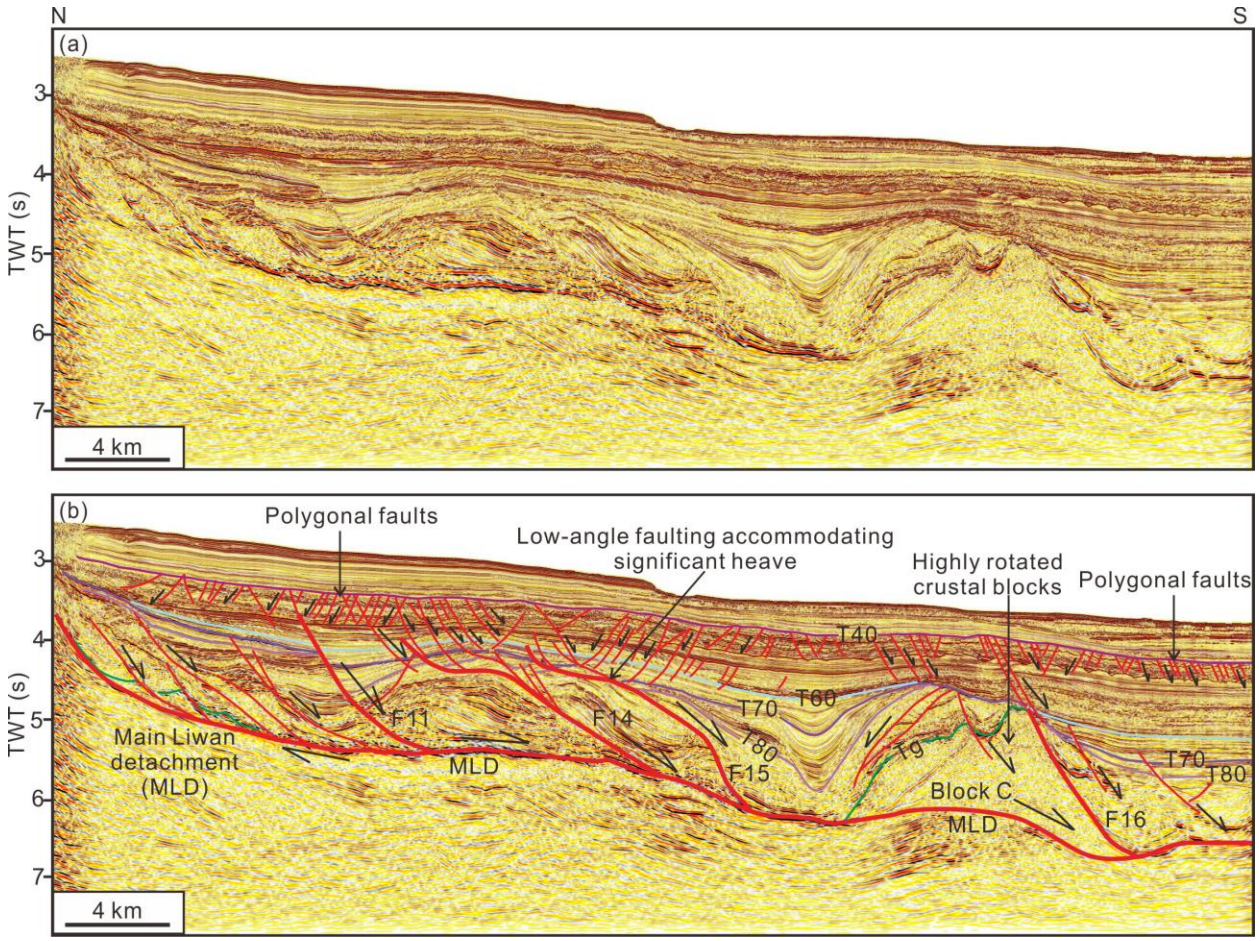

Figure 5. (a) Uninterpreted and (b) Interpreted north-south profile 500 from the central part of the 3D seismic volume. Location of the seismic profile is shown in Figure 1c.

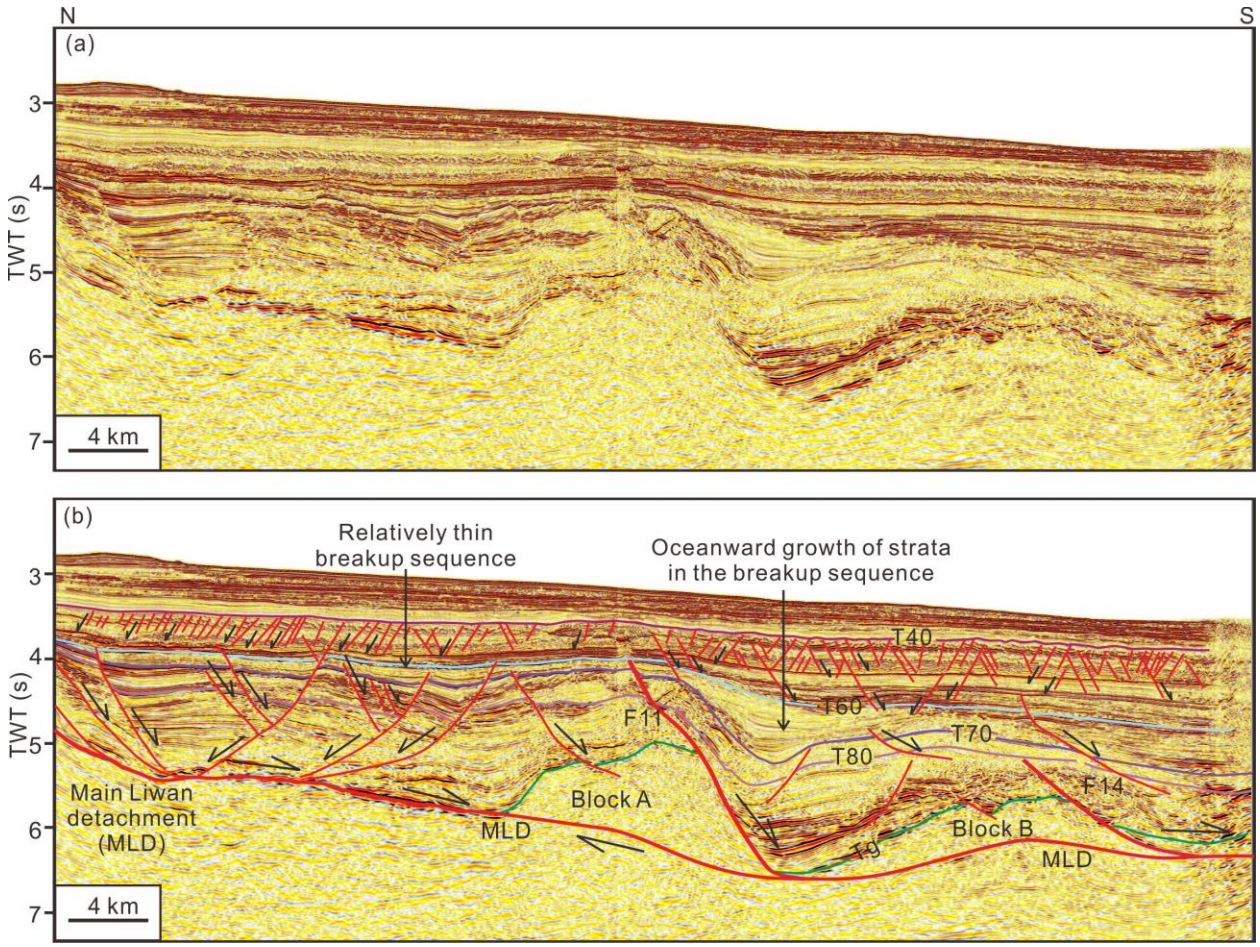

Figure 6. (a) Uninterpreted and (b) Interpreted north-south profile 370 from the western part of the 3D seismic volume. Location of the seismic profile is shown in Figure 1c.

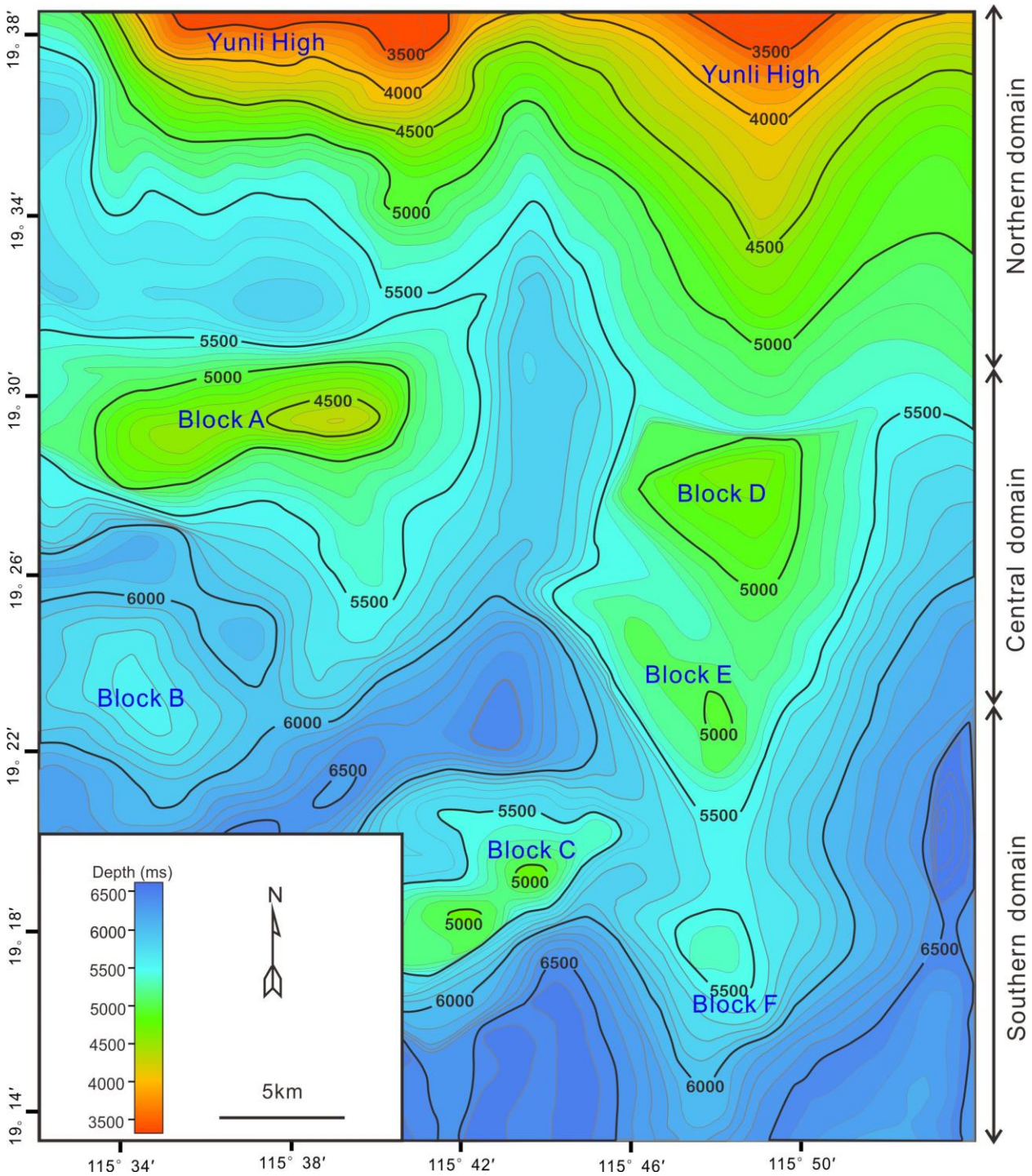

Figure 7. Depth map of Horizon Tg, marking the boundary between crystalline basement and Cenozoic sediment. The depth map shows a complex basement topography comprising several structural highs. Note that we divided the Liwan Sub-basin into northern, central and southern domains in order to describe their specific structural and depositional histories.

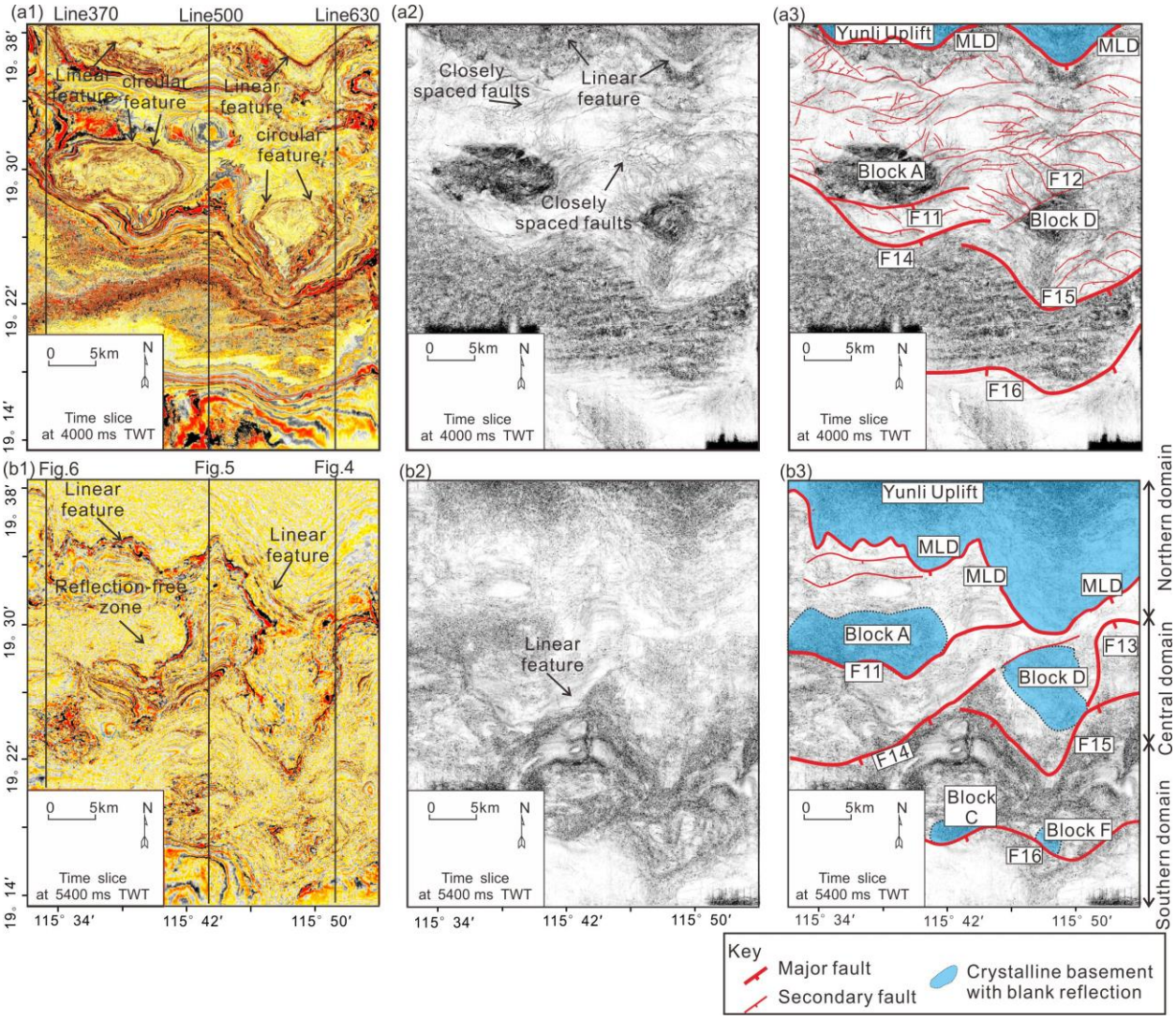

Figure 8. Time and coherence slices extracted from the 3D seismic volume at a depth of 4000 ms TWT (a1-a3) and 5400 ms TWT (b1-b3). Figures a3 and b3 shows the structures interpreted from the time and coherence slices. MLD: Main Liwan Detachment. F: fault.

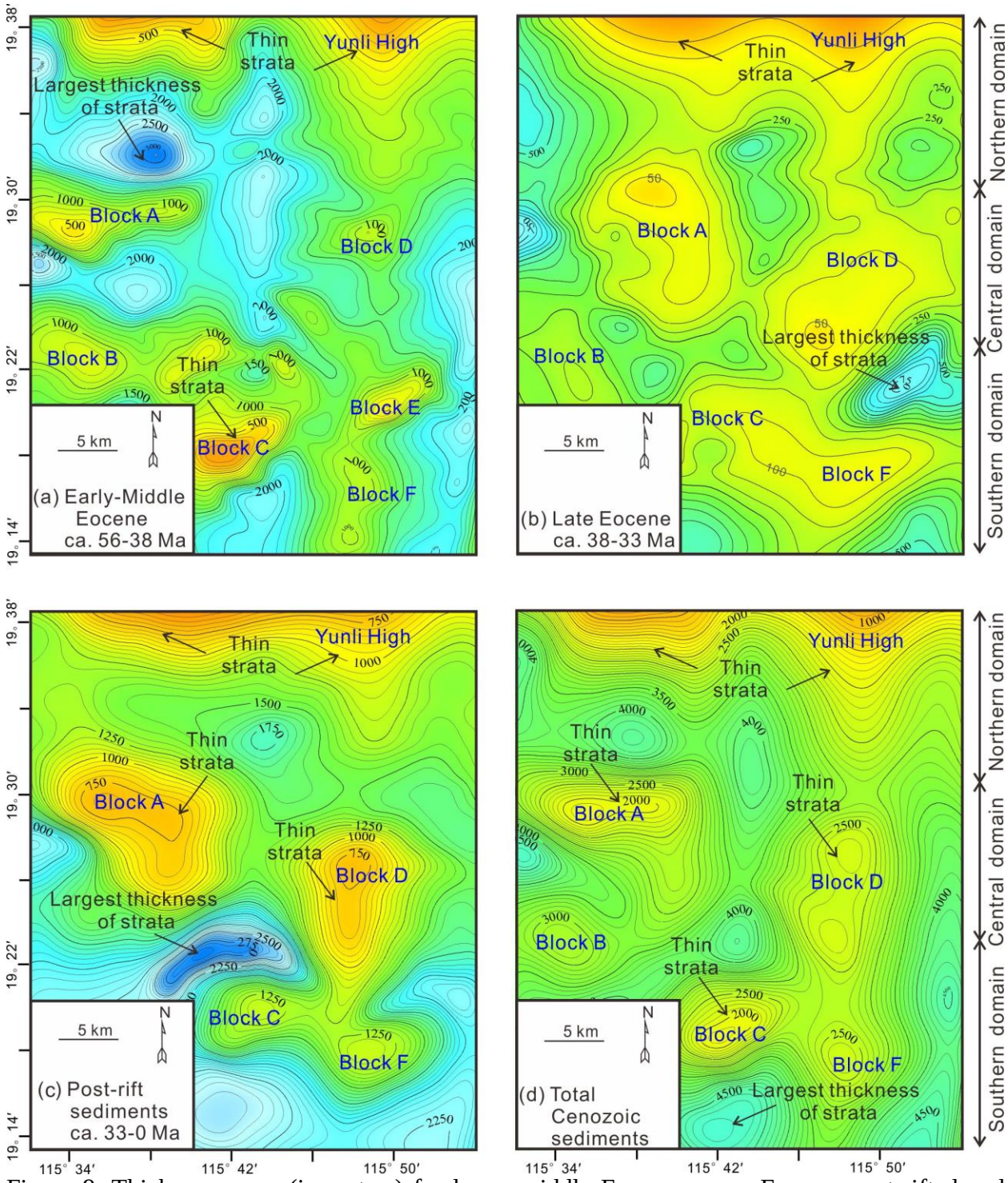

Figure 9. Thickness maps (in metres) for lower-middle Eocene, upper Eocene, post-rifted and Cenozoic strata in the Liwan Sub-basin. The maps illustrate thickness variations associated with specific time periods referred to in this work.

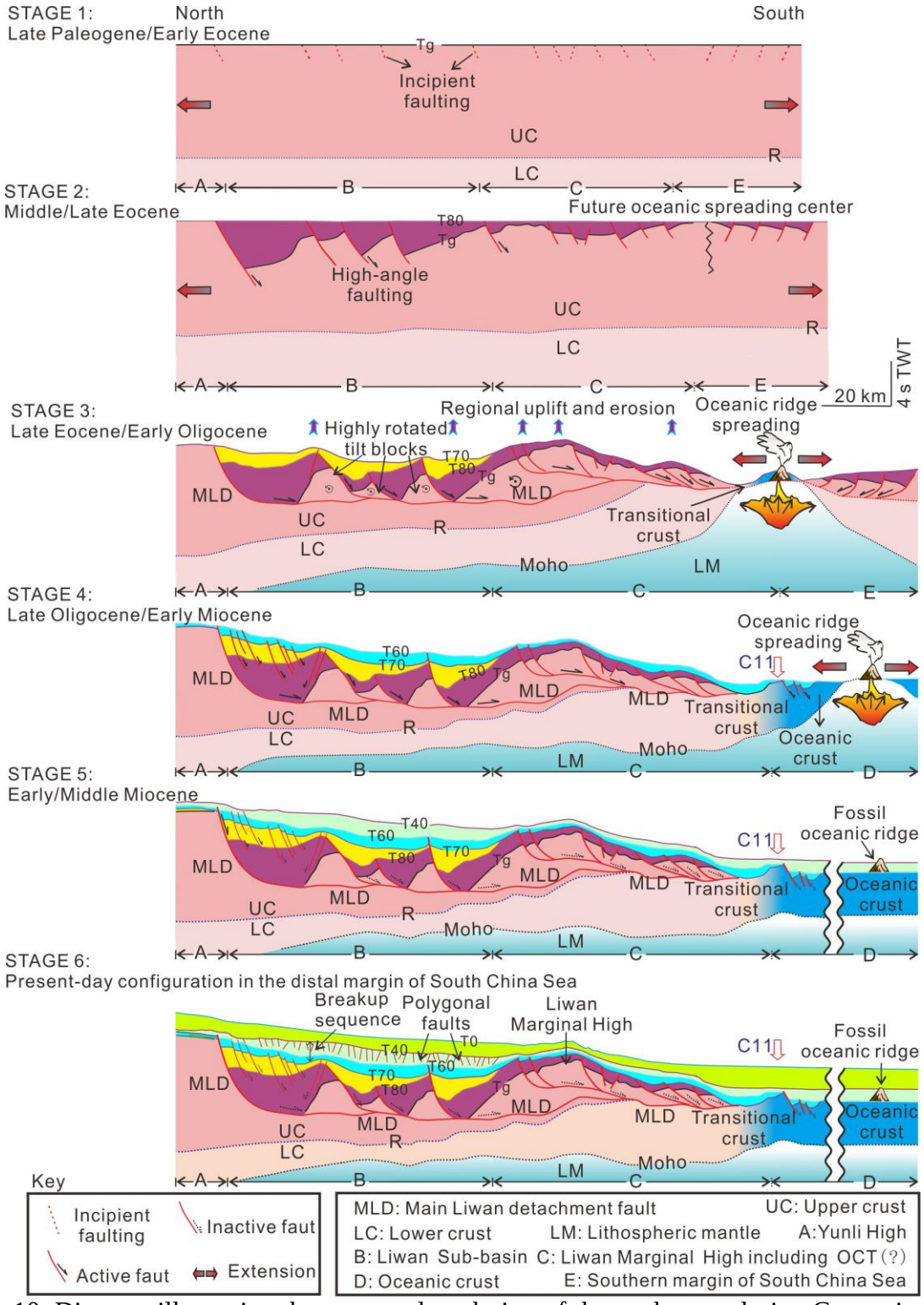

Figure 10. Diagram illustrating the structural evolution of the study area during Cenozoic rifting and continental breakup, northern South China Sea. See text for a detailed explanation of the figure.

	Block A	Block B	Block C	Block D	Block E	Block F
Area (km^2)	64.9	37.3	26.9	32.6	28.3	32.8
Width (km)	4.8	4.4	5.9	5.4	5.3	5.2
Length (km)	15.2	12.5	7.5	8.7	9.2	10.2

Table 1. Geometry of rotated tilt blocks in the Liwan Sub-basin.